Band Gap Tuning and Defect Tolerance of Atomically Thin Two- Dimensional Organic-Inorganic Halide Perovskites

Pandey, Mohnish; Jacobsen, Karsten Wedel; Thygesen, Kristian Sommer

Published in:
Journal of Physical Chemistry Letters

Link to article, DOI:
10.1021/acs.jpclett.6b01998

Publication date:
2016

Document Version
Peer reviewed version

Band Gap Tuning and Defect Tolerance of Atomically Thin Two-Dimensional Organic-Inorganic Halide Perovskites

Mohnish Pandey,*,† Karsten W. Jacobsen,† and Kristian S. Thygesen†,‡

Center for Atomic-scale Materials Design (CAMD), Department of Physics, Technical University of Denmark, DK - 2800 Kongens Lyngby, Denmark, and Center for Nanostructured Graphene (CNG), Department of Physics, Technical University of Denmark, DK - 2800 Kongens Lyngby, Denmark

E-mail: mohpa@fysik.dtu.dk

*To whom correspondence should be addressed

†Center for Atomic-scale Materials Design (CAMD), Department of Physics, Technical University of Denmark, DK - 2800 Kongens Lyngby, Denmark

‡Center for Nanostructured Graphene (CNG), Department of Physics, Technical University of Denmark, DK - 2800 Kongens Lyngby, Denmark

Abstract

Organic-inorganic halide perovskites have proven highly successful for photovoltaics, but suffer from low stability which deteriorates their performance over time. Recent experiments have demonstrated that low dimensional phases of the hybrid perovskites may exhibit improved stability. Here we report first-principles calculations for isolated monolayers of the organometallic halide perovskites $(C_4H_9NH_3)_2MX_2Y_2$ where M=Pb, Ge, Sn and X,Y=Cl, Br, I. The band gaps computed using the GLLB-SC functional are found to be in excellent agreement with experimental photoluminescence data for the already synthesised perovskites. Finally, we study the effect of different defects on the band structure. We find that the most common defects only introduce shallow or no states in the band gap indicating that these atomically thin two-dimensional perovskites are likely to be defect tolerant.

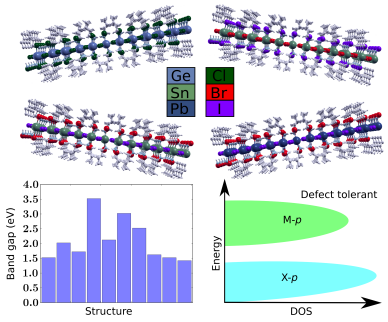

Over the past five years photovoltaic (PV) devices based on organic-inorganic halide perovskites have undergone an unprecedented increase in power conversion efficiency (PCE).[1–3] Most notably, the $MAPbI_3$ (MA: methylammonia) perovskite with a band gap of 1.5 eV, strong light absorption, and long photocarrier lifetimes, has been demonstrated in several solar cell architectures with above 15% PCE.[4,5] Very recently a PCE above 20% efficiency was reported by combining $MAPbBr_3$ with $FAPbI_3$ (FA: formamidinium).[6] Two major disadvantages of these materials are that they contain toxic lead (Pb) and are unstable in contact with moisture which may lead to pronounced defect formation, dissociation or mechanical failure.[7] The replacement of lead by tin (Sn) has been found to yield PCEs of up to 6%, but worsens the stability. A number of Pb-free perovskite oxides, e.g. $BiFeO_3$,

$BiMnO_3$ and $BiFe_2CrO_6$, were found to have improved stability compared to the halides but also significantly lower efficiencies.[8,9] Finding ways of overcoming the stability issues of the hybrid halide perovskites without compromising their PCE remains the main obstacle for using these materials as basis for a viable PV technology.

Interestingly, two-dimensional (2D) phases of the hybrid halide perovskites have been shown to have better stability than the $MAPbI_3$ like bulk phases (due to a release of geometric constraints as expressed by the Goldschmidt tolerance factor) and significant efforts are presently being made to synthesize and characterize these novel materials.[10–16] The atomically thin 2D hybrid perovskites can be synthesised in solution and are thus relatively simple to produce compared to many other atomically thin 2D materials which are made by mechanical exfoliation or by chemical vapour/atomic layer deposition.[15,17] Furthermore, the atomically thin 2D regime of the hybrid perovskites provides unique opportunities for tuning the electronic structure e.g. by substrate interactions, mechanical strain, quantum confinement (layer thickness), stacking of different atomically thin 2D crystals to create van der Waals heterostructures[18] or by varying the size of the alkyl chains.[19] The bottom-up approach recently demonstrated for a layer-by-layer synthesis of the atomically thin 2D perovskites has opened up a new frontier to synthesize and tailor the properties of these compounds.[15,20] Moreover, recent work by Liu *et. al* has demonstrated that the properties of the defects occurring in the low-dimensional hybrid perovskites can be controlled via the synthesis conditions.[21]

In this Article, we use first principles calculations to explore different derivatives of the atomically thin 2D lead perovskites reported experimentally in Ref. 15. We stress that the calculations are performed for isolated monolayers of the layered perovskites. In the following we use the terms monolayer and 2D perovskites interchangeably. Specifically we investigate the effect of mixing different halogen atoms and substituting lead with germanium and tin as previously been demonstrated experimentally for the bulk perovskites.[22] The substitution of the lead atoms with germanium or tin not only provides an avenue for lead-free perovskites

but is also way to modify the electronic structure, e.g. the size of the band gap. We find that Pb-substitution by Sn and Ge generally lowers the band gaps from the 2.5-3.5 eV range to the 1.7-2.5 eV range which is more relevant for single and multi-junction solar cells and photoluminscence applications. Additionally, we find that all the 2D perovskites explored in our work have direct band gaps and have low carrier effective masses which are a prerequisites for efficient light absorption and good transport properties, respectively. We also explore the effect of halogen and metal-halide vacancies on the band structure, in particular whether they introduce deep or shallow states. We find that all the 2D perovskites largely preserve their band structure upon introducing different vacancy defects indicating a strong degree of tolerance to defects.

All the electronic structure calculations were performed using density functional theory (DFT) as implemented in the GPAW code.[23] For accurate calculations of lattice constants the PBEsol functional[24] was used and the atomic geometry was optimized with the BEEF-vdW functional[25] to account for the van der Waals forces between the organic parts of the monolayers. The monolayers were separated by 15 Å vacuum to avoid interactions due to the periodic boundary conditions. The Kohn-Sham single particle energy gap along with the derivative discontinuity and the spin-orbit coupling was calculated with the GLLB-SC functional[26,27] which yields much improved band gaps for both bulk[28] and 2D semiconductors[29] as compared to semi-local functionals. The atomic structure of the pristine materials as well as the materials with the defects were relaxed until the forces were below 0.05 eV/Å. Using a more strict convergence criterion of 0.02 eV/Å for a prototypical system (Rb_2GeI_4) changes the energy by less than 1 meV per unit cell, and therefore we used the criterion 0.05 eV/Å to lower the computational cost. The position of the defect levels were estimated from the Kohn-Sham single particle band structure applying Slater-Janak transition state theory for an accurate description of localised states in the band gap.[30] The initial guess for the atomic structure of the 2D perovskites (see Figure 1) was taken from the Ref. 15. It should be noted that only the bulk structure is provided in Ref. 15. We thus extracted the struc-

ture of a monolayer from the bulk to create the 2D perovskites. The different compounds were then generated by elemental substitution and full atomic and unit cell relaxations were carried out for all the structures. The z-direction of the unit cell was kept fixed in order to preserve the vacuum between the monolayers.

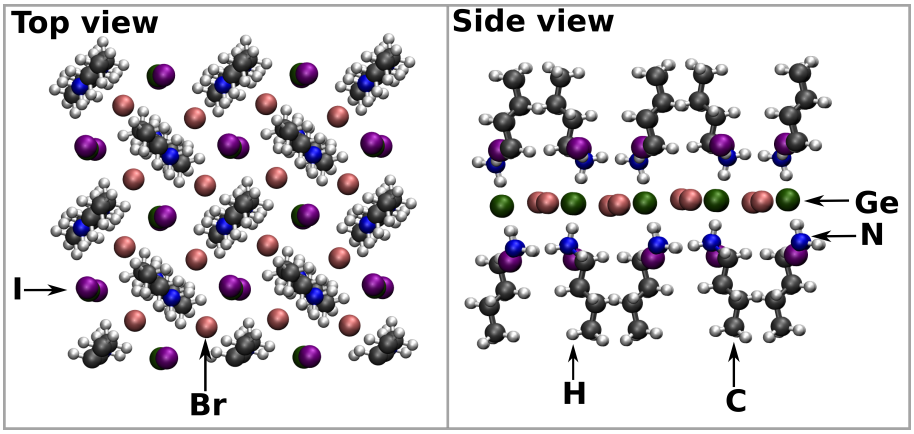

Figure 1: Top and side view of the monolayer $A_2GeBr_2I_2$ (A = $C_4H_9NH_3$) perovskite, respectively.

Figure 2 shows the calculated band gaps of the 27 monolayer perovskites $A_2MX_2Y_2$ (A = $C_4H_9NH_3$, M=Sn, Ge, Pb; X, Y=Cl, Br, I). Since the mixed halides have different halogen atoms in the axial and equatorial positions, they are represented with different letters 'X' and 'Y'. In Figure 2, for brevity the organic part (A) is omitted from the chemical formula on the x-axis. The first element represents the metal atom and the second and third elements represent the equatorial and axial halogen atoms, respectively. The band gaps shown in Figure 2 have been calculated with and without spin-orbit coupling (SOC). As expected, SOC has the largest effect on the band structure of the lead containing perovskites where it lowers the band gaps by around 1 eV due to splitting of the conduction band which consists mainly of Pb p-states. The experimental values for the band gaps are from Refs. 15 and 22. The band gaps are clearly different when the halogen atoms from the axial and equatorial positions are swapped. This behavior can be intuitively understood in terms of ionic radii of the halogen atoms. The ionic radii increases in the order Cl, Br, I and the in-plane

lattice parameters are mainly governed by the ions within plane i.e. the equatorial position. Therefore, the chlorine atoms in the equatorial plane give the smallest lattice constant and the iodine atoms the largest. The splitting of the energy levels in the stretched lattice is not so pronounced thus giving smaller band gaps as compared to the more compressed lattice where the splitting of the energy levels is larger. Consequently, smaller halogen atoms within the plane lead to larger band gaps.

In Ref. 15 the band gap of some of the Pb-based perovskites was calculated using the PBE xc-functional without inclusion of spin-orbit coupling. Our results indicate that the reasonable agreement with experiments highlighted in that work is fortuitous. Indeed, the PBE xc-functional underestimates the band gap and inclusion of SOC would yield a band gap around 1 eV smaller than the experimental value. The inclusion of the derivative discontinuity by the GLLBSC functional increases the band gap by around 1 eV restoring the excellent agreement with experiments. In addition, deviations from the DFT calculations in Ref. 15 are expected because our structure optimizations were performed using a van der Waals xc-functional.

Our DFT-GLLBSC calculations predict the band gaps of the isolated monolayers to be larger than the layered bulk phase by 0.1-0.2 eV. This is again in good agreement with the experiments in Ref. 15 which found the position of the photoluminescence peak of the A_2PbBr_4 perovskite to increase by 0.05 eV when going from bulk to the 3-layer thick perovskite film. We mention that optical properties of 2D semiconductors, like the transition metal dichalcogenides, typically show a strong dependence on the film thickness. This dependence is due to (i) quantum confinement effects, i.e. interlayer hybridisation, which can affect the qualitative feature of the band structure such as the nature of the band gap (whether direct or indirect) and (ii) the strong reduction of the dielectric screening properties when the film thickness is reduced towards the monolayer.[31] Our calculations show that the effect of quantum confinement is very weak. This is clearly a result of the relatively large distance between the perovskite layers, resulting from the large size of the organic cations. We have

not attempted to compute the difference in the dielectric function of the bulk and monolayers due to the large computational demands of such calculations for the 78 atom unit cells, and postpone a more detailed investigation of the electron-hole interaction and excitonic effects in these materials to a future study.

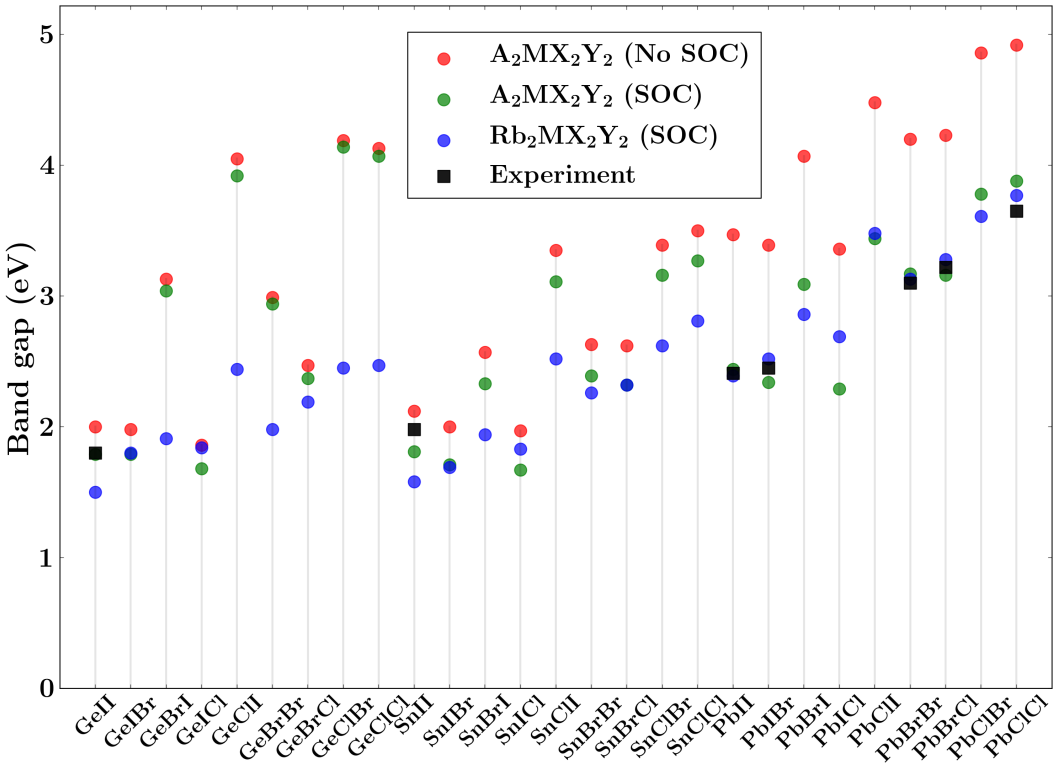

Figure 2: The calculated band gaps of the the monolayers with and without the spin-orbit interaction denoted by 'SOC' and 'No SOC', respectively. The compounds are arranged in the order of the perovskites containing Ge, Sn and Pb respectively. The order for halogen atoms is taken as I, Br and Cl. The compounds with the swapped position of the halogen atoms are placed next to each other for comparing the effect of the swapping on the band gap. The names of the compounds are abbreviated in such a way that the first element represents the metal atom and the second and third element represent the in-plane and axial halogen atoms respectively. The experimental values of the band gaps are taken from ref. 15 and 22.

Apart from the size of the band gap, the shape and nature of the bands, especially near the band edges, also plays a crucial role in governing the electronic properties. Bands with larger curvature leads to lower effective carrier masses which is desirable for high mobility of the charge carriers. The orbital character of the bands near the band edges determine

the optical absorption strength and, to some extent, control the defect properties of the material.[21,30,32,33] Figure 3 (a) shows the PBE band structure of a representative compound, A_2PbI_4, plotted along a high symmetry path. The figure clearly shows that A_2PbI_4 has a direct band gap at the center of the Brillouin zone (Γ-point). In addition, the large curvature of the band edge states implies low effective masses of the charge carriers, see Table 1 for the numerical values of the effective masses. We should stress that we are referring to the in-plane effective mass of the isolated 2D monolayer; the out-of-plane effective masses of the layered bulk perovskites are practically infinite. The character of the bands of A_2PbI_4 near the band edges can be seen in the projected density of states (PDOS) plotted in Figure 3 (b). The valence band and conduction band edge states are mainly dominated by iodine p and lead p states, respectively. The significantly different character of the valence and conduction band edge states allude to high ionicity of A_2PbI_4.[21] The remaining 26 compounds have qualitatively similar band structures, i.e. direct band gap at the Γ-point, low effective masses, and different orbital character of the band edge states.

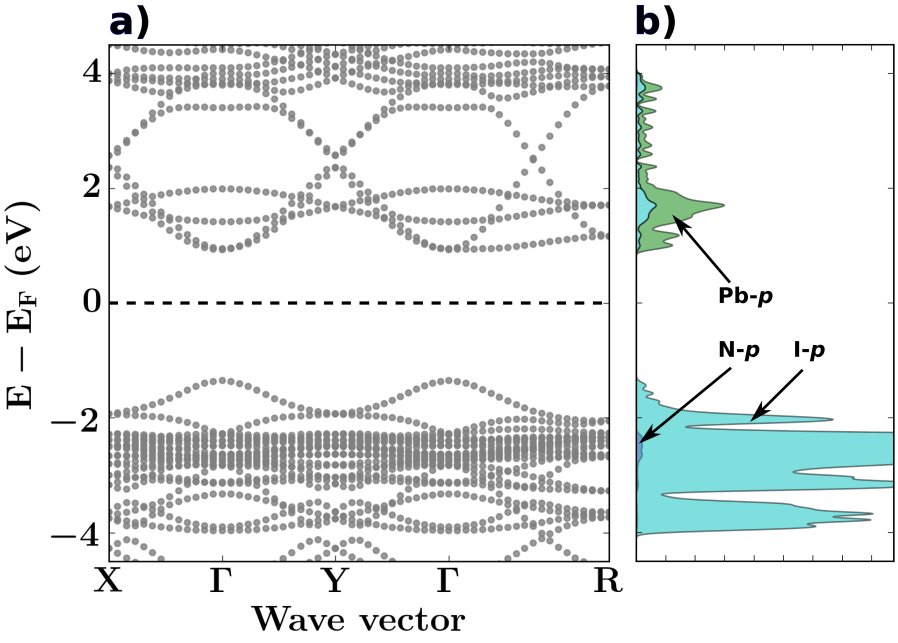

Figure 3: a) PBE band structure of a representative compound, A_2PbI_4 plotted along a high symmetry path. b) The density of states (in arbitrary units) projected onto atomic orbitals.

Table 1: The band gaps and carrier effective masses. The compounds are named in the same way as in Figure 2. m_e^* and m_h^* denote the electron and hole effective masses, respectively. For the sake of completeness the band gaps (E_g) from Figure 2 are also mentioned in the table.

Compound	m_e^*	m_h^*	E_g	Compound	m_e^*	m_h^*	E_g	Compound	m_e^*	m_h^*	E_g
GeII	0.14	0.14	1.79	SnII	0.17	0.18	1.81	PbII	0.26	0.22	2.44
GeIBr	0.13	0.20	1.79	SnIBr	0.15	0.17	1.71	PbIBr	0.23	0.21	2.34
GeBrI	0.35	0.25	3.04	SnBrI	0.21	0.19	2.33	PbBrI	0.39	0.25	3.09
GeICl	0.13	0.19	1.68	SnICl	0.14	0.19	1.67	PbICl	0.20	0.20	2.29
GeClI	0.80	0.30	3.92	SnClI	0.33	0.32	3.11	PbClI	0.68	0.31	3.44
GeBrBr	0.22	0.23	2.94	SnBrBr	0.19	0.23	2.39	PbBrBr	0.28	0.26	3.17
GeBrCl	0.15	0.24	2.37	SnBrCl	0.18	0.24	2.32	PbBrCl	0.26	0.26	3.16
GeClBr	0.44	0.36	4.14	SnClBr	0.26	0.32	3.16	PbClBr	0.39	0.32	3.78
GeClCl	0.34	0.36	4.07	SnClCl	0.26	0.34	3.27	PbClCl	0.34	0.31	3.88

From a computational point of view, the large size of the organic molecules renders the study of defects in the 2D organometallic perovskites rather demanding. At the same time, it is known from the bulk perovskites that the organic molecules are typically not directly involved in the formation of the bands closest to the Fermi energy, see Figure 3 (a). This suggest that it may be possible to replace the organic molecule by a simpler anion without altering the qualitative features of the electronic structure. Focusing on the particular case of 2D lead perovskites, Liu *et al.* demonstrated with their calculations that the organic part in the 2D perovskites can be substituted by rubidium (Rb) atoms without affecting the electronic properties significantly.[21] We have explored the effect of replacing the organic molecule by Rb for all the 27 compounds. We find that in most of the cases of lead-containing perovskites this is an excellent approximation. However, we also find that for many tin and germanium perovskites, and for some of the lead perovskites, the substitution underestimates the band gap significantly, see Figure 2. This mainly arises from differences in the atomic structure of $A_2MX_2Y_2$ and $Rb_2MX_2Y_2$. Apart from the change in the band gap induced by strain effects, the organic part distorts the octahedral coordination environment which has

the effect of enlarging the band gap.[34] Therefore, the different band gaps of $A_2MX_2Y_2$ and $Rb_2MX_2Y_2$ is a combined effect of the distortion and the difference in lattice constants of the two structures. However, to the best of our knowledge no experimental study has been carried out for monolayer $Rb_2MX_2Y_2$ perovskites.

Despite being structurally different and (as a consequence) introduce changes in the size of the band gap, the rubidium substitution does not alter the nature of the states near the valence band maximum (VBM) and the conduction band minimum (CBM). In particular, the organic part in $A_2MX_2Y_2$ and rubidium in $Rb_2MX_2Y_2$ do not contribute to the states near the band edges,[21] see Figure 4 a&b. The VBM and CBM are mainly

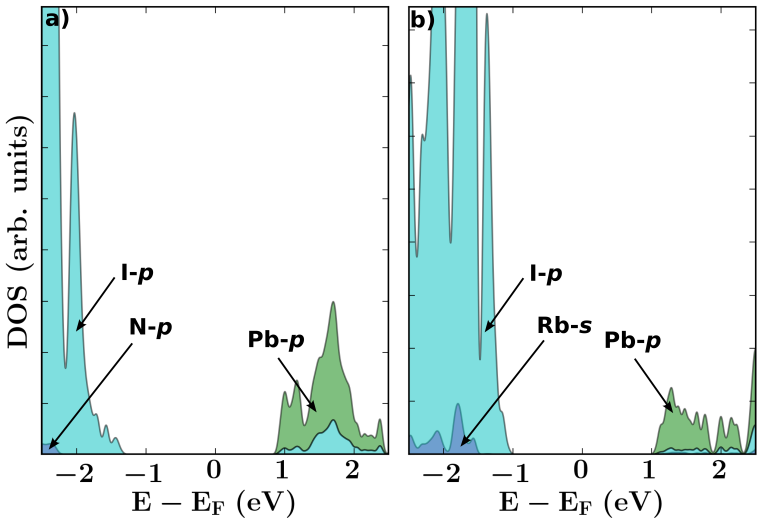

Figure 4: (a) PDOS for A_2PbI_4. (b) PDOS for Rb_2PbI_4

composed of X-p and M-p states, respectively. This indicates that the VBM has an anti-bonding character whereas the CBM is bonding in nature. The relationship between the nature of the PDOS and their bonding and antibonding character has been established in our earlier work for the case of 2D transition metal dichalcogenides.[30] Briefly, we have shown that the tendency of a 2D semiconductor to form mid-gap states upon introducing vacancy defects can be quantitatively described by the similarity of the states composing the band edges. The degree of similarity is estimated using a normalized orbital overlap (NOO)

which measures the bonding/antibonding character of the VBM and CBM edge states.[30] The average character of the edge states are described by an orbital fingerprint vector,[30]

$$\alpha = c(\rho_{\nu_1}, \rho_{\nu_2}, .., \rho_{\nu_N}) \tag{1}$$

where c is a normalization constant, ν_i are combined atom and angular momentum channel indices and ρ_{ν_i} is the corresponding PDOS integrated over an energy window at either the bottom of the conduction band or the top of the valence band. The normalized orbital overlap, D, between the valence and conduction band edge states is then defined as the inner product between the orbital fingerprint vector of the conduction and valence bands. Semiconductors with an NOO value close to 1 (indicating a bonding-antibonding nature of the band gap) have stronger tendency to form deep gap states upon introducing vacancies compared to semiconductors with D values significantly less than 1 which tend to form only shallow gap states.

Since the nature of the PDOS of $A_2MX_2Y_2$ and $Rb_2MX_2Y_2$ is similar near the band edges, both classes of materials are expected to possess similar defect properties with regard to the formation of deep/shallow gap states. In particular, from Figure 4 it is clear that both classes of materials have significantly different orbital character of the VBM and CBM and thus we expect low NOO and large tolerance towards defects. Figure 5 shows the NOO values of the 2D halides $A_2MX_2Y_2$ and $Rb_2MX_2Y_2$. For reference, the NOO values of MoS_2 and WS_2 are also shown. These two materials are known to form deep gap states upon formation of sulfur vacancies. The figure clearly shows that all 2D perovskites have significantly lower values of NOO as compared to the defect sensitive dichalcogenides. As expected from Figure 4, the $A_2MX_2Y_2$ and $Rb_2MX_2Y_2$ structures have very similar NOO values, indicating that the tendency to form defect states is also very similar for the two classes of materials.

Figure 6 shows the DOS of A_2PbI_4 (a)-(c) and Rb_2PbI_4 (d)-(f) monolayers in the pristine

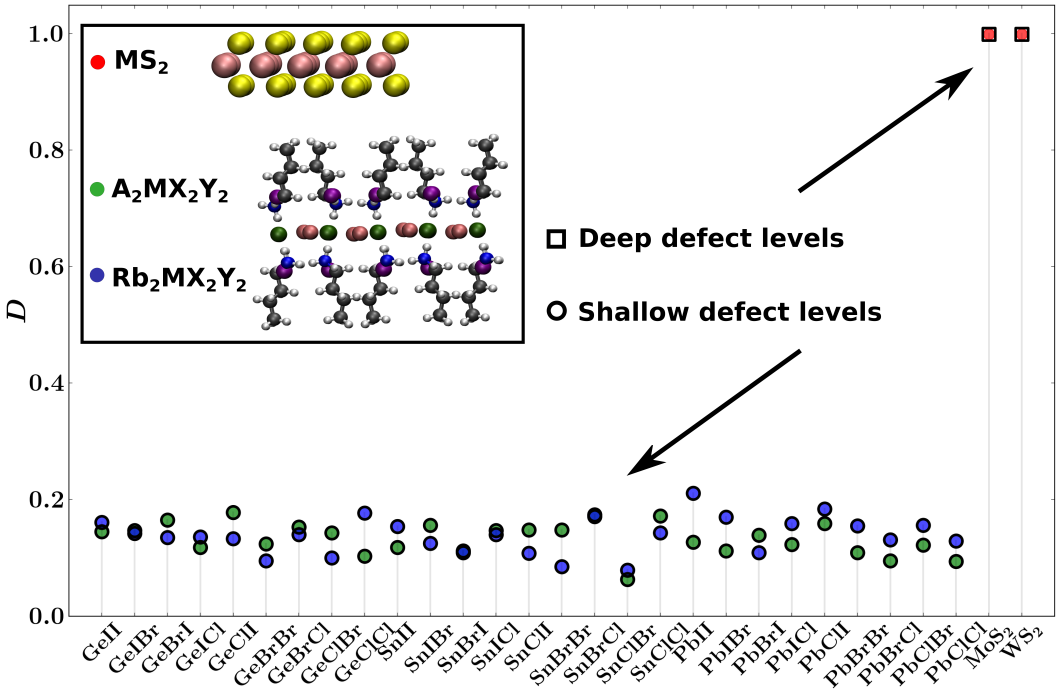

Figure 5: Normalized orbital overlap (NOO) to measure the similarity of the states near the VBM and CBM edges.[30] The NOO values for the MoS_2 and WS_2 monolayers are also shown (red circles) for comparison. The band edge states in MoS_2 and WS_2 have very similar character thus giving high NOO values whereas the significantly different nature of the edge states in $A_2MX_2Y_2$ and $Rb_2MX_2Y_2$ gives low NOO values (gree and blue circles, respectively) for these class of materials.

form and with defects. The three panels of Figure 6 (a)-(c) and (d)-(f) correspond to the pristine materials, the materials with a halogen vacancy in the axial position and with a halogen vacancy in the equatorial position, respectively. The systems with the vacancies have been calculated with half an electron less in order to get reasonable estimates of the defect level from the Kohn-Sham band structure as per the Slater-Janak theory.[30,35] The figure clearly shows that both A_2PbI_4 and Rb_2PbI_4 introduce shallow gap states close to the CBM. Similar behaviors can be expected for other types of defects, e.g. PbI_2 and RbI (or AI) vacancies. Unfortunately, for the $A_2MX_2Y_2$ monolayers these more complex defects are computationally quite challenging because of the large supercells required to remove the defect-defect interactions. We therefore focus on the simpler $Rb_2MX_2Y_2$ compounds when exploring larger defects, but expect the results to be representative also for the $A_2MX_2Y_2$ compounds due to their qualitatively similar electronic structure.

Figure 7 shows the the DOS of a lead-free perovskite monolayer, Rb_2GeBr_4. Panel (a) denotes the pristine monolayer while (b) and (c) correspond to the monolayer with a halogen atom removed from the axial and equatorial position, respectively. Panels (d) and (e) correspond to the monolayer with a $GeBr_2$ and RbI vacancy, respectively. The figure clearly shows that no deep gap states are formed upon introducing any of these different types of vacancy defects Similar behavior is observed for the other 26 monolayer perovskites (see Supporting Information). The behavior of preserving the band structure upon creating the defects is a clear manifestation of defect tolerance in these 2D perovskites corroborating with the inferences from Figure 5. Additionally, the similarity of the electronic structure of the $A_2MX_2Y_2$ and $Rb_2MX_2Y_2$ compounds suggests that similar behavior can be expected for other 2D perovskites with different organic chains or metal atoms.

Finally, we have investigated the thermodynamic stability of the $A_2MX_2Y_2$ and $Rb_2MX_2Y_2$ mixed halide 2D perovskites by calculating the energy of segregation into the pure per-

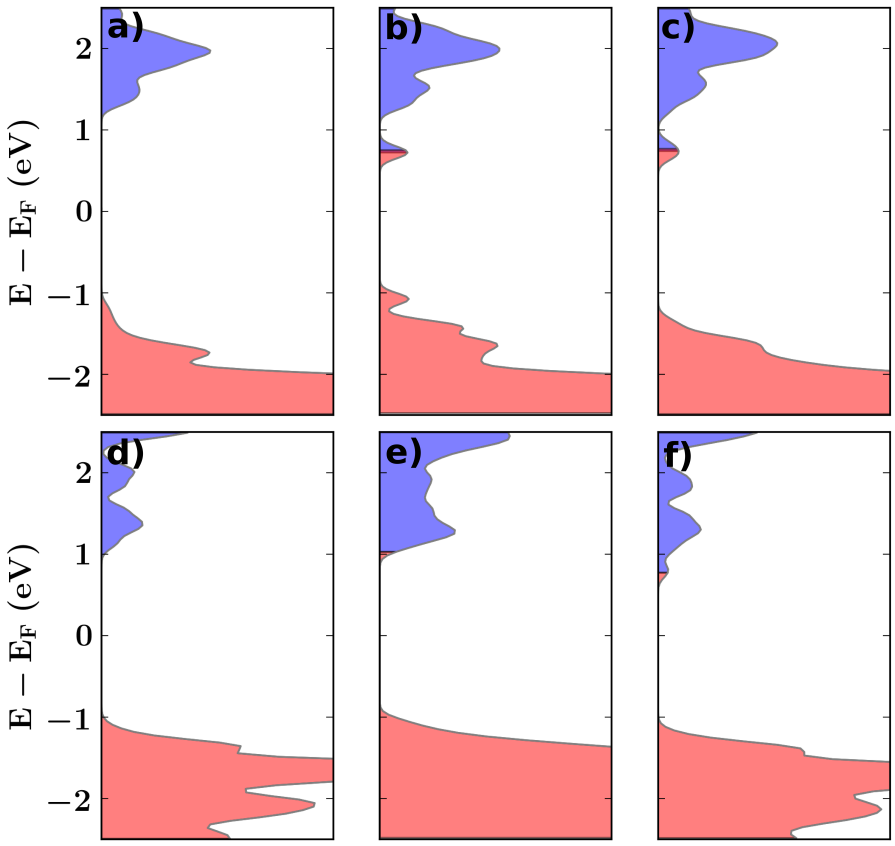

Figure 6: The DOS plots of A_2PbI_4 in the panels a-c correspond to the pristine, halogen vacancy in the axial position and the halogen vacancy in the equatorial position, respectively. The panels d-f show the similar plot as a-c for Rb_2PbI_4. Red color denotes the states filled up to the Fermi level while the blue color denotes the unoccupied states.

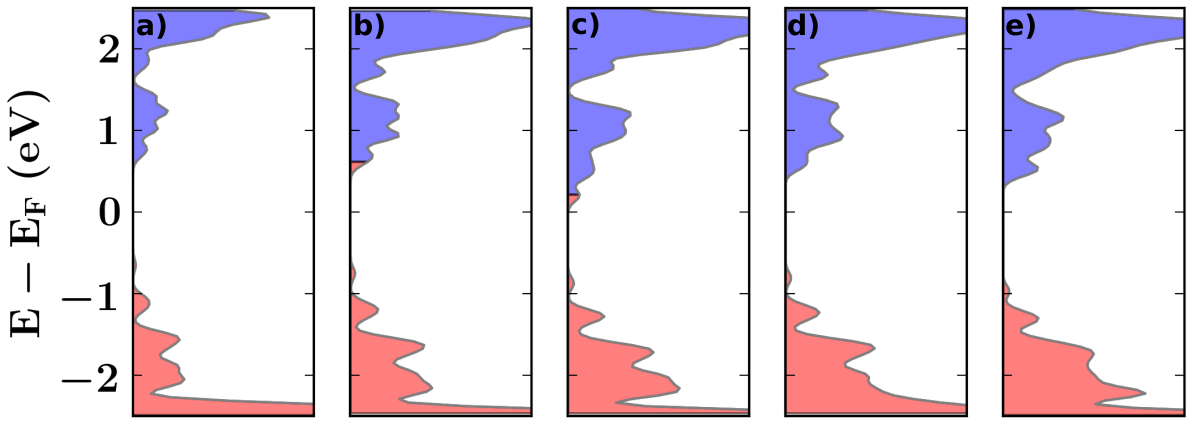

Figure 7: The DOS plot of Rb_2GeBr_4. (a) denotes the pristine monolayer; b) and c) correspond to the monolayer with halogen atom removed from the axial and equatorial position, respectively; d) and e) correspond to the monolayer with $GeBr_2$ and RbI vacancy, respectively. Red color denotes the states filled up to the Fermi level while the blue color denotes the unoccupied states.

ovskites,

$$\Delta H^{segr} = E[A_2MX_2Y_2] - \frac{1}{2}(E[A_2MX_4] + E[A_2MY_4]) \quad (2)$$

where ΔH^{segr} is the heat of segregation and E represents the calculated total energy of the compound. The same expression is used to calculate the segregation energy of $Rb_2MX_2Y_2$. The calculated ΔH^{segr} is shown in Figure 8. A significant number of the compounds have negative value of ΔH^{segr} indicating that the mixed phase is thermodynamically stable. We stress that inclusion of entropic effects (not considered here) would stabilise the mixed phases under finite temperature conditions. Furthermore, the positive ΔH^{segr} values are not too large implying that the structures may be metastable. This aspect was previously explored for the bulk hybrid pervoskites.[36]

In summary, the 2D hybrid perovskites explored in the present work show remarkable properties of relevance for various opto-electronic applications. In particular, the lead-free perovskites with direct band gaps in the range 1.7-2.5 eV, low charge carrier effective masses, and high defect tolerance are promising candidates for photovoltaics. The preservation of

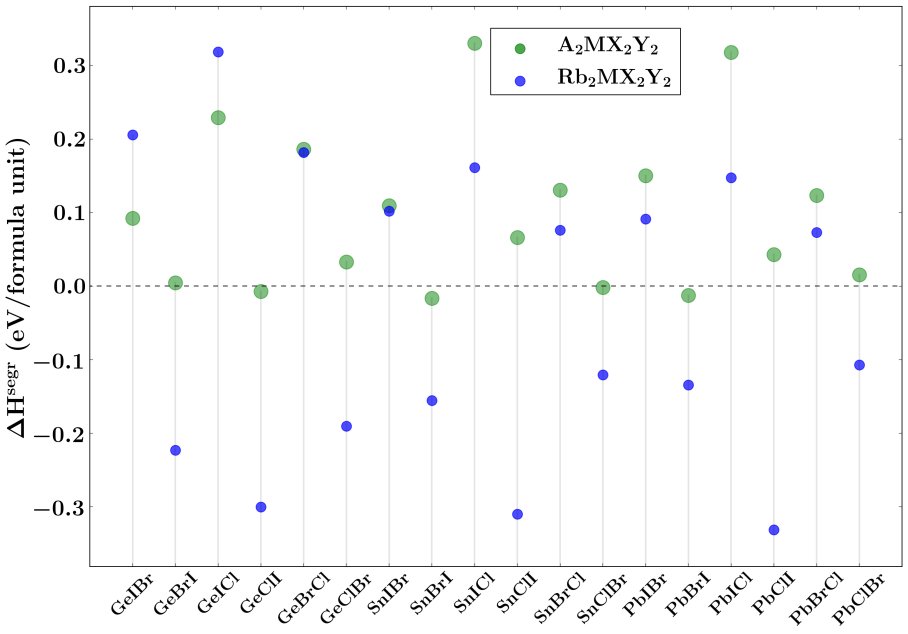

Figure 8: Calculated segregation energy (ΔH^{segr}) of mixed halide 2D perovskites $A_2MX_2Y_2$ and $Rb_2MX_2Y_2$ to pure phases.

the band structure with respect to the creation of different vacancy defects was shown to be the result of the bonding/anti-bonding nature of the conduction and valence band states, respectively. We also found that the function of the organic chains is not only to donate electrons to the metal-halogen cage but also to distort the cubic symmetry. By comparing to the much simpler cubic Rb-substituted perovskites, it was found that this symmetry breaking has the effect of enlarging the band gap. However, apart from this Rb-substitution does not affect the qualitative features of the electronic states near the band edges. This indicates that the band gap and optical properties of the 2D hybrid perovskites can be further tuned by varying the organic chains without compromising its defect tolerance.

Acknowledgments

The Center for Nanostructured Graphene is sponsored by the Danish National Research Foundation, Project DNRF103. This work was partly supported by a research grant (9455) from VILLUM FONDEN.

The Supporting Information:

Band structures of 27 2D perovskites and the density of states plots of the pristine structures and the structures with different vacancy defects. This material is available free of charge via the Internet at http://pubs.acs.org.

References

(1) Nie, W.; Tsai, H.; Asadpour, R.; Blancon, J.-C.; Neukirch, A. J.; Gupta, G.; Crochet, J. J.; Chhowalla, M.; Tretiak, S.; Alam, M. A.; *et al.*, High-Efficiency Solution-Processed Perovskite Solar Cells with Millimeter-Scale Grains. *Science* **2015**, *347*, 522–525.

(2) Zhou, H.; Chen, Q.; Li, G.; Luo, S.; Song, T.-b.; Duan, H.-S.; Hong, Z.; You, J.; Liu, Y.; Yang, Y. Interface Engineering of Highly Efficient Perovskite Solar Cells. *Science* **2014**, *345*, 542–546.

(3) Pellet, N.; Gao, P.; Gregori, G.; Yang, T.-Y.; Nazeeruddin, M. K.; Maier, J.; Grätzel, M. Mixed-Organic-Cation Perovskite Photovoltaics for Enhanced Solar-Light Harvesting. *Angew. Chem. Int. Ed.* **2014**, *53*, 3151–3157.

(4) Eperon, G. E.; Stranks, S. D.; Menelaou, C.; Johnston, M. B.; Herz, L. M.; Snaith, H. J. Formamidinium Lead Trihalide: A Broadly Tunable Perovskite for Efficient Planar Heterojunction Solar Cells. *Energy Environ. Sci.* **2014**, *7*, 982–988.

(5) Kim, H.-S.; Lee, C.-R.; Im, J.-H.; Lee, K.-B.; Moehl, T.; Marchioro, A.; Moon, S.-J.; Humphry-Baker, R.; Yum, J.-H.; Moser, J. E.; *et al.*, Lead Iodide Perovskite Sensitized All-Solid-State Submicron Thin Film Mesoscopic Solar Cell with Efficiency Exceeding 9%. *Sci. Rep.* **2012**, *2*, 591.

(6) Jeon, N. J.; Noh, J. H.; Yang, W. S.; Kim, Y. C.; Ryu, S.; Seo, J.; Seok, S. I. Compositional Engineering of Perovskite Materials for High-Performance Solar Cells. *Nature* **2015**, *517*, 476–480.

(7) Stranks, S. D.; Snaith, H. J. Metal-Halide Perovskites for Photovoltaic and Light-Emitting Devices. *Nat. Nanotechnol.* **2015**, *10*, 391–402.

(8) Chakrabartty, J. P.; Nechache, R.; Harnagea, C.; Rosei, F. Photovoltaic Effect in Multiphase Bi-Mn-O Thin Films. *Opt. Express* **2014**, *22*, A80–A89.

(9) Grinberg, I.; West, D. V.; Torres, M.; Gou, G.; Stein, D. M.; Wu, L.; Chen, G.; Gallo, E. M.; Akbashev, A. R.; Davies, P. K.; *et al.*, Perovskite Oxides for Visible-Light-Absorbing Ferroelectric and Photovoltaic Materials. *Nature* **2013**, *503*, 509–512.

(10) Boix, P. P.; Agarwala, S.; Koh, T. M.; Mathews, N.; Mhaisalkar, S. G. Perovskite Solar Cells: Beyond Methylammonium Lead Iodide. *J. Phys. Chem. Lett.* **2015**, *6*, 898–907.

(11) Smith, I. C.; Hoke, E. T.; Solis-Ibarra, D.; McGehee, M. D.; Karunadasa, H. I. A Layered Hybrid Perovskite Solar-Cell Absorber with Enhanced Moisture Stability. *Angew. Chem. Int. Ed.* **2014**, *53*, 11232–11235.

(12) Cao, D. H.; Stoumpos, C. C.; Farha, O. K.; Hupp, J. T.; Kanatzidis, M. G. 2D Homologous Perovskites as Light-Absorbing Materials for Solar Cell Applications. *J. Am. Chem. Soc.* **2015**, *137*, 7843–7850.

(13) Koh, T. M.; Shanmugam, V.; Schlipf, J.; Oesinghaus, L.; Müller-Buschbaum, P.; Ramakrishnan, N.; Swamy, V.; Mathews, N.; Boix, P. P.; Mhaisalkar, S. G. Nanostructuring Mixed-Dimensional Perovskites: A Route Toward Tunable, Efficient Photovoltaics. *Adv. Mater. 28*, 3653–3661.

(14) Sichert, J. A.; Tong, Y.; Mutz, N.; Vollmer, M.; Fischer, S.; Milowska, K. Z.; Cortadella, R. G.; Nickel, B.; Cardenas-Daw, C.; Stolarczyk, J. K.; *et al.*, Quantum Size Effect in Organometal Halide Perovskite Nanoplatelets. *Nano Lett.* **2015**, *15*, 6521–6527.

(15) Dou, L.; Wong, A. B.; Yu, Y.; Lai, M.; Kornienko, N.; Eaton, S. W.; Fu, A.; Bischak, C. G.; Ma, J.; Ding, T.; *et al.*, Atomically Thin Two-Dimensional Organic-Inorganic Hybrid Perovskites. *Science* **2015**, *349*, 1518–1521.

(16) Quan, L. N.; Yuan, M.; Comin, R.; Voznyy, O.; Beauregard, E. M.; Hoogland, S.; Buin, A.; Kirmani, A. R.; Zhao, K.; Amassian, A.; *et al.*, Ligand-Stabilized Reduced-Dimensionality Perovskites. *J. Am. Chem. Soc.* **2016**, *138*, 2649–2655.

(17) Niu, W.; Eiden, A.; Vijaya Prakash, G.; Baumberg, J. J. Exfoliation of Self-Assembled 2D Organic-Inorganic Perovskite Semiconductors. *App. Phys. Lett.* **2014**, *104*, 171111.

(18) Geim, A. K.; Grigorieva, I. V. Van der Waals Heterostructures. *Nature* **2013**, *499*, 419–425.

(19) González-Carrero, S.; Galian, R. E.; Pérez-Prieto, J. Organometal Halide Perovskites: Bulk Low-Dimension Materials and Nanoparticles. *Part. Part. Syst. Charact.* **2015**, *32*, 709–720.

(20) Liu, J.; Xue, Y.; Wang, Z.; Xu, Z.-Q.; Zheng, C.; Weber, B.; Song, J.; Wang, Y.; Lu, Y.; Zhang, Y.; *et al.*, Two-Dimensional $CH_3NH_3PbI_3$ Perovskite: Synthesis and Optoelectronic Application. *ACS Nano* **2016**, *10*, 3536–3542.

(21) Liu, Y.; Xiao, H.; Goddard, W. A. Two-Dimensional Halide Perovskites: Tuning Electronic Activities of Defects. *Nano Lett.* **2016**, *16*, 3335–3340.

(22) Mitzi, D. B. Synthesis, Crystal Structure, and Optical and Thermal Properties of $(C_4H_9NH_3)_2MI_4$ (M = Ge, Sn, Pb). *Chem. Mater.* **1996**, *8*, 791–800.

(23) Enkovaara, J.; Rostgaard, C.; Mortensen, J. J.; Chen, J.; Dułak, M.; Ferrighi, L.; Gavnholt, J.; Glinsvad, C.; Haikola, V.; Hansen, H. A.; *et al.*, Electronic Structure Calculations with GPAW: A Real-Space Implementation of the Projector Augmented-wave Method. *J. Phys.: Condens. Matter* **2010**, *22*, 253202.

(24) Perdew, J. P.; Ruzsinszky, A.; Csonka, G. I.; Vydrov, O. A.; Scuseria, G. E.; Constantin, L. A.; Zhou, X.; Burke, K. Restoring the Density-Gradient Expansion for Exchange in Solids and Surfaces. *Phys. Rev. Lett.* **2008**, *100*, 136406.

(25) Wellendorff, J.; Lundgaard, K. T.; Møgelhøj, A.; Petzold, V.; Landis, D. D.; Nørskov, J. K.; Bligaard, T.; Jacobsen, K. W. Density Functionals for Surface Science: Exchange-Correlation Model Development with Bayesian Error Estimation. *Phys. Rev. B* **2012**, *85*, 235149.

(26) Gritsenko, O.; van Leeuwen, R.; van Lenthe, E.; Baerends, E. J. Self-Consistent Approximation to the Kohn-Sham Exchange Potential. *Phys. Rev. A* **1995**, *51*, 1944.

(27) Kuisma, M.; Ojanen, J.; Enkovaara, J.; Rantala, T. T. Kohn-Sham Potential with Discontinuity for Band Gap Materials. *Phys. Rev. B* **2010**, *82*, 115106.

(28) Castelli, I. E.; Hüser, F.; Pandey, M.; Li, H.; Thygesen, K. S.; Seger, B.; Jain, A.; Persson, K. A.; Ceder, G.; Jacobsen, K. W. New Light-Harvesting Materials Using Accurate and Efficient Bandgap Calculations. *Adv. Ener. Mater.* **2015**, *5*, 1400915.

(29) Rasmussen, F. A.; Thygesen, K. S. Computational 2D Materials Database: Electronic Structure of Transition-Metal Dichalcogenides and Oxides. *J. Phys. Chem. C* **2015**, *119*, 13169–13183.

(30) Pandey, M.; Rasmussen, F. A.; Kuhar, K.; Olsen, T.; Jacobsen, K. W.; Thygesen, K. S. Defect-Tolerant Monolayer Transition Metal Dichalcogenides. *Nano Lett.* **2016**, *16*, 2234–2239.

(31) Latini, S.; Olsen, T.; Thygesen, K. S. Excitons in van der Waals Heterostructures: The Important Role of Dielectric Screening. *Phys. Rev. B* **2015**, *92*, 245123.

(32) Dirin, D. N.; Protesescu, L.; Trummer, D.; Kochetygov, I. V.; Yakunin, S.; Krumeich, F.; Stadie, N. P.; Kovalenko, M. V. Harnessing Defect-Tolerance at the Nanoscale: Highly Luminescent Lead Halide Perovskite Nanocrystals in Mesoporous Silica Matrixes. *Nano Lett. 16*, 5866–5874.

(33) Steirer, K. X.; Schulz, P.; Teeter, G.; Stevanovic, V.; Yang, M.; Zhu, K.; Berry, J. J. Defect Tolerance in Methylammonium Lead Triiodide Perovskite. *ACS Ener. Lett.* **2016**, *1*, 360–366.

(34) Gao, W.; Gao, X.; Abtew, T. A.; Sun, Y.-Y.; Zhang, S.; Zhang, P. Quasiparticle Band Gap of Organic-Inorganic Hybrid Perovskites: Crystal Structure, Spin-Orbit Coupling, and Self-Energy Effects. *Phys. Rev. B* **2016**, *93*, 085202.

(35) Li, Y.; Sanna, S.; Schmidt, W. G. Modeling Intrinsic Defects in $LiNbO_3$ within the Slater-Janak Transition State Mode. *J. Chem. Phys.* **2014**, *140*, 234113.

(36) Nagabhushana, G.; Shivaramaiah, R.; Navrotsky, A. Direct Calorimetric Verification of Thermodynamic Instability of Lead Halide Hybrid Perovskites. *Proc. Natl. Acad. Sci. U. S. A.* **2016**, *113*, 7717–7721.